Directly photoinscribed refractive index change and Bragg gratings in Ohara WMS-15 glass ceramic

Peter A. Krug,* Rodica Matei Rogojan, and Jacques Albert

Department of Electronics, Carleton University, 1125 Colonel By Drive, Ottawa, Ontario K1S 5B6, Canada

*Corresponding author: pkrug@doe.carleton.ca

Received 12 January 2009; revised 15 May 2009; accepted 16 May 2009;
posted 19 May 2009 (Doc. ID 106092); published 11 June 2009

We inscribed thick volume gratings in WMS-15 glass ceramic by ultraviolet light at 193 and 248 nm. Unlike earlier work in ceramic materials, the inscription process modified the optical properties of the material without the need for any additional chemical or thermal processing. Experimental evidence from measurements of grating growth, thermal annealing, and spectral absorption indicates that two distinct physical mechanisms are responsible for the grating formation. Weak, easily thermally bleached gratings resulted from exposure fluences below $0.3\,kJ/cm^2$. Optical absorption measurements suggest that these low fluence gratings are predominantly absorption gratings. More thermally stable gratings, found to be refractive index gratings with unsaturated refractive index modulation amplitude as large as 6×10^{-5} were formed at cumulative fluences of $1\,kJ/cm^2$ and above. © 2009 Optical Society of America

OCIS codes: 050.7330, 160.2750, 160.5335, 230.1480.

1. Introduction

Glass ceramics are composite materials obtained by the controlled nucleation and crystallization of glass [1]. Glass ceramics combine many useful properties, which can include small or negative thermo-optic coefficient, transparency or opacity, robustness, and machinability [2]. The thermal expansion coefficient of glass ceramics can vary widely from negative values [3,4] to virtually zero [5] to $1.40 \times 10^{-6}/°C$ [6] at or near room temperature.

Traditionally, the optical applications of glass ceramics were limited to uses such as mirror substrates, where the low optical transparency of available glass ceramics was not an issue. High optical transparency is achieved in glass ceramics either when the crystalline and glass phases have closely matched refractive indices, or the crystals are substantially smaller than a wavelength of light, or both. The optical absorption of the glass and crystalline phases must also be small. Recently, glass ceramics that are sufficiently transparent to be used in transmissive optical components have been reported and have become available commercially [2,5,7]. Glass ceramics are now being investigated for optical applications including laser host materials [8–10] and saturable absorbers [11,12].

It is well known that irradiation with intense ultraviolet (UV) light can cause permanent refractive index changes in many types of glass. Refractive index changes induced with periodic or quasi-periodically patterned beams can inscribe permanent diffraction gratings and holograms in bulk glass [13], in planar waveguides, and in optical fibers [14,15]. Optically induced, permanent change in refractive index has been studied in many different glass hosts. Important parameters in grating inscription include the sign, size, and rate of growth of the refractive index change, the ease of generation of that index change, and its thermal and long-term stability. Mechanical and thermal properties of the glass also are important in the application of structures and devices created by photoinduced index change. There is great interest in the exploration of new photosensitive optical materials, especially when those materials have combinations of optical, mechanical, or thermal properties not available in known photosensitive materials. Thermally stable

0003-6935/09/183429-09$15.00/0
© 2009 Optical Society of America

volume gratings find applications in many optical systems, including interferometers, sensors, and laser resonators [16]. There is particular interest in the creation of diffraction gratings and volume holograms in glass ceramics because of their unique thermal properties [1,2].

Stookey was the first to report photosensitivity in glass-ceramic materials as long ago as 1949 [17]. He demonstrated photoinduced opacity in metal-doped glasses and glass ceramics that were subsequently heated. Photoetchable glass ceramics, such as Schott Foturan, allow fabrication of complex shaped structures by UV exposure, followed by chemical etching [18–20]. Diffraction gratings have been optically written in photothermorefractive (PTR) glass using UV exposure followed by thermal treatment [21–23]. Efimov *et al.* [24] showed that the photosensitivity of these PTR glasses arises when cerium atoms are ionized by the UV photons, and the electrons released in the process neutralize silver ions, which upon thermal processing then diffuse and cluster in the form of silver nanocrystals. Chiodini *et al.* [25,26] reported unpatterned permanent changes in the refractive index of tin-silicate glass ceramic exposed to UV radiation. Paleari *et al.* [27] reported refractive index patterning in a tin-silicate glass ceramic using an 800 nm femtosecond laser.

In this paper we report, for the first time to our knowledge, the direct photoinscription of volume diffraction gratings in a glass ceramic without the need for any subsequent processing.

2. UV Inscription of Gratings

Conventional photosensitivity requires that the writing wavelength be either in the long wavelength tail of the UV absorption edge of the material, or else near a color center band in the UV. We selected Ohara WMS-15 transparent glass ceramic [28,29] because data provided by the manufacturer indicates that this glass ceramic has small but nonzero optical transmission at the 248 nm emission wavelength of a KrF excimer laser. The composition range of WMS-15 is given in Table 1.

The plane-polished WMS-15 glass-ceramic samples were 3 mm thick. In a first series of exposures at 248 nm, these samples were exposed through a phase mask to a 2.5 mm × 2.5 mm uniform beam with an energy density of 226 mJ/cm^2 per pulse, at a repetition rate of 25 pulses per second. The peak power density during the excimer laser pulses was around 10 MW/cm^2. We varied the irradiation time to expose the samples to total ultraviolet doses ranging from 0.01 to 30 kJ/cm^2.

Table 1. Chemical Composition Range of Ohara WMS-15 Glass Ceramic as Reported by the Manufacturer [29]

Chemical Species	Percentage by Weight
SiO_2	70–80
Al_2O_3	2–10
ZrO_2	2–10
P_2O_5	2–10
ZnO	0–2
Sb_2O_3	0–2

The phase mask period was 886.2 nm, and its groove depth was optimized for maximum first-order diffraction efficiency and zero-order beam suppression at 248 nm. During the irradiation, the mask was in direct physical contact with one polished face of the glass-ceramic sample.

We measured the diffraction efficiency of the gratings using a collimated, TE polarized, 1 mm diameter 632.8 nm wavelength beam from a 15 mW helium–neon laser. The laser was incident on each grating at the Bragg angle, $\theta_B = \sin^{-1}(\lambda/2\Lambda)$, where $\lambda = 632.8$ nm is the illuminating wavelength and $\Lambda = 443.1$ nm is the period of the grating. For these gratings, the Bragg angle was 45.6°. We measured the diffraction efficiency, defined by $\eta = P_{\text{diffracted}}/P_{\text{incident}}$, where $P_{\text{diffracted}}$ is the power of the first-order Bragg diffracted beam and P_{incident} is the power incident on the front surface of the grating. All optical powers were measured by an optical power meter with an 11.3 mm diameter sensitive area. The diffraction efficiency as a function of UV dose is shown in Fig. 1.

In Fig. 1 we see that there are two very distinctly different regions of grating formation. For UV doses less than 1 kJ/cm^2, we observe the formation of weak gratings, having diffraction efficiency of less than 2×10^{-5}. These gratings reach maximum strength at the relatively low dose of 0.03 kJ/cm^2, after which their strength decreases with increasing dose up to 1 kJ/cm^2. For UV doses above 1 kJ/cm^2, much stronger grating growth is observed, with the gratings continuing to grow with increasing UV dose up to the maximum applied dose of 30 kJ/cm^2. The strongest grating in the high-UV-dose regime, written at 30 kJ/cm^2, has a diffraction efficiency of 2.3×10^{-3},

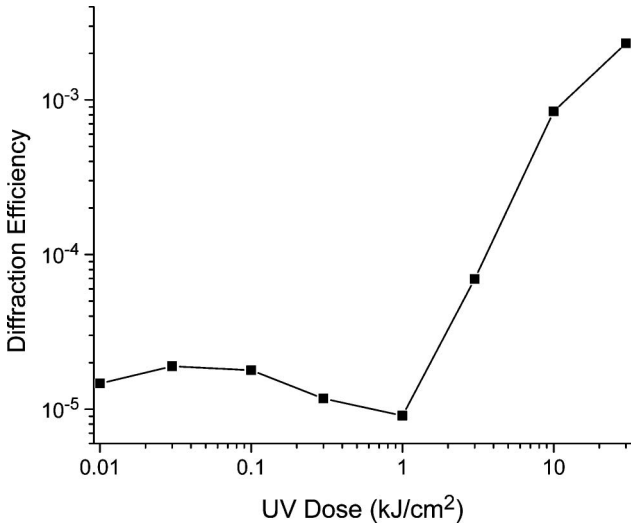

Fig. 1. Diffraction efficiency as a function of UV dose (which we define as fluence integrated over the entire exposure), for gratings written at 248 nm.

which is more than 100 times the efficiency of the strongest grating in the low UV dose regime.

The depth of a thick holographic grating can be determined from the measured angular dependence of the diffraction efficiency. For the $30\,\mathrm{kJ/cm^2}$ grating, Fig. 2 shows the dependence of η on the angular detuning $\Delta\theta = \theta_B - \theta$, where θ is the incidence angle of the probe beam on the grating.

Kogelnik shows, using coupled-mode theory for thick refractive index gratings, that the thickness of a grating, d, is related to the angular half- power bandwidth of the angular detuning curve, $2\Delta\theta_{1/2}$, by [30]

$$d \approx \frac{\Lambda}{2\Delta\theta_{1/2}}. \tag{1a}$$

From an empirical Lorentzian fit to the data in Fig. 2, we obtained $2\Delta\theta_{1/2} = 0.20°$. Using Eq. (1a), we calculate the thickness of the $30\,\mathrm{kJ/cm^2}$ grating to be $127 \pm 20\,\mu\mathrm{m}$. A similar measurement shows that the thickness of the $0.03\,\mathrm{kJ/cm^2}$ grating is $254 \pm 20\,\mu\mathrm{m}$. Alternatively, for reasons explained in Section 4, we must also consider the possibility that the low fluence gratings are predominantly absorption gratings. Then the relationship between d and $\Delta\theta_{1/2}$ is given by [30]

$$d \approx \frac{1.5\lambda}{2\Delta\theta_{1/2}\pi n \sin\theta_B}. \tag{1b}$$

Using a measured value of $2\Delta\theta_{1/2} = 0.10°$ and $n = 1.524$, we find $d \approx 160\,\mu\mathrm{m}$.

The decreased thickness of the strong grating is discussed in Section 4, where we consider the change in optical absorption associated with the UV exposure of the glass ceramic.

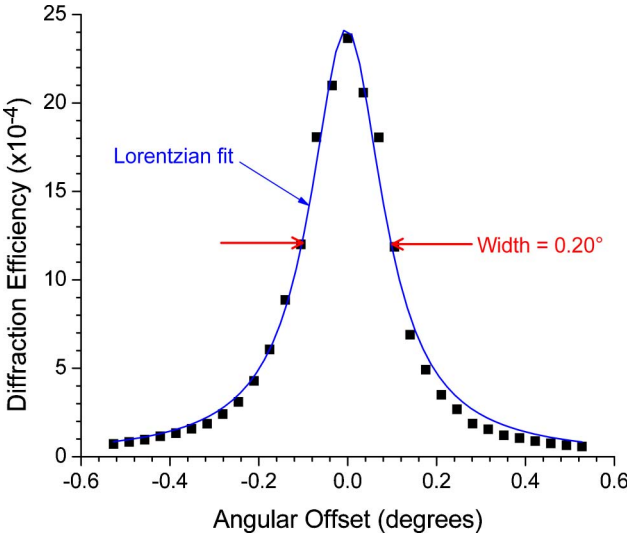

Fig. 2. (Color online) Diffraction efficiency versus incident beam angular offset from the Bragg angle. The squares are measured, and the continuous curve is an empirical Lorentzian fit to the data. The grating was written with $30\,\mathrm{kJ/cm^2}$ at 248 nm.

For the high-fluence grating, we can use the measured grating thicknesses to calculate the refractive index modulation amplitude corresponding to the measured diffraction efficiency, by rearranging Kogelnik's Eq. 45 [30]:

$$\Delta n = \frac{\lambda \cos\theta_B}{\pi\, d} \arcsin\sqrt{\eta}. \tag{2}$$

The diffraction efficiency, η, was corrected to take into account the Fresnel reflections from the two surfaces of the substrate. The index modulation amplitude for the grating written at $30\,\mathrm{kJ/cm^2}$ was 5.6×10^{-5}. The limit of detection of the diffracted beam is estimated to correspond to about $\Delta n \approx 3 \times 10^{-7}$.

We initially chose 248 nm as the inscription wavelength because its optical absorption depth in the WMS-15 glass ceramic is many wavelengths (see Section 4), allowing us to write thick gratings. In a second series of exposures, we also wrote several gratings using the 193 nm ArF excimer line, whose absorption depth is much smaller. The gratings were written at energy doses 0.03, 0.3, 3, and $30\,\mathrm{kJ/cm^2}$, and at a repetition rate of 100 pulses per second. Heating of the substrate at the higher repetition rate (we previously used 25 pulses per second for the 248 nm writing) was not a significant concern, because the energy per pulse was 5 times lower than for the gratings written at 248 nm. We used a phase mask optimized for 193 nm illumination. The period Λ of the gratings written by this mask was 335.4 nm.

He–Ne laser side diffraction measurements showed that gratings were formed at all energy doses. From the half-power bandwidth of the angular detuning curve of the diffracted beam (Eq. (1a)) we estimated the thickness of the $30\,\mathrm{kJ/cm^2}$ grating to be $8.5\,\mu\mathrm{m}$. To ensure that it is valid to apply Kogelnik's thick grating theory for these thinner gratings, we calculate Kogelnik's thickness parameter [30]:

$$Q = \frac{2\pi\lambda d}{n\Lambda^2}. \tag{3}$$

Substituting the estimated grating thickness, we find that $Q \approx 200$, which easily satisfies the thick grating criterion $Q \gg 1$.

From Eq. (2), and using $d = 8.5\,\mu\mathrm{m}$ we calculated the index modulation amplitude. The results, shown in Fig. 3, are compared with the index modulation amplitude for the gratings written at 248 nm.

For the high-dose gratings, we see that there is little difference between the index modulation amplitude induced at 193 and 248 nm, despite the very different depth of penetration of the UV light into the glass-ceramic substrate. This suggests that the grating formation may be associated with a structural rearrangement of the glass and crystal phases, not necessarily associated with a particular atomic, ionic, or molecular absorption band in the material. For

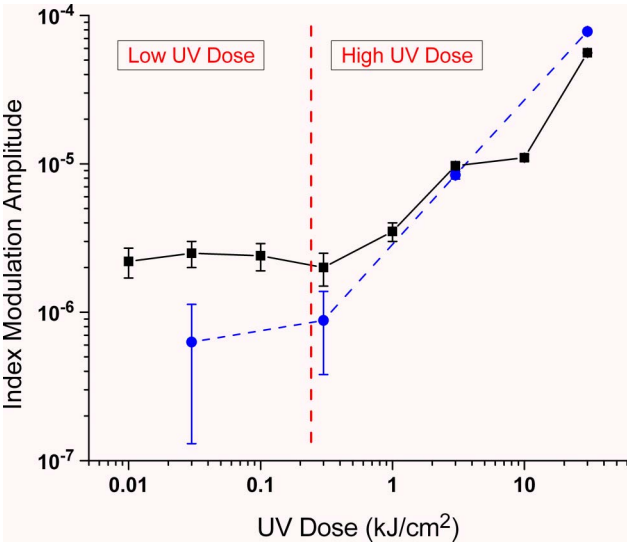

Fig. 3. (Color online) Refractive index modulation depth for gratings written at 248 nm (squares) and 193 nm (circles). The dashed vertical line divides the low- and high-UV-dose regimes.

the low-energy dose exposures, the gratings written at 193 nm were very weak and, consequently, the estimated error bars on the points are large enough to make it futile to compare the index modulation amplitude with that measured in the gratings written at 248 nm.

3. Annealing of Gratings

The stability of photoinscribed gratings at elevated temperatures and over long times is very important in practical applications. Furthermore, thermally induced changes in grating strength can throw light on the grating formation mechanisms. We annealed the gratings at temperatures ranging from 100 to 500 °C, as shown in Table 2.

The diffraction efficiency as a function of UV dose following each annealing stage is shown in Fig. 4. For grating diffraction efficiencies below 10^{-6}, measurement uncertainties became very large, and no measurement was possible for $\eta < 2 \times 10^{-7}$ (corresponding to $\Delta n \approx 3 \times 10^{-7}$) as above. In the low-UV-dose regime, we see that the gratings become progressively weaker with each stage of annealing. To make the annealing behavior easy to follow, in Fig. 5 we show the same data, plotted as diffraction efficiency versus annealing stage, with a separate curve for each UV exposure dose. For UV doses below 1 kJ/cm², no measurable grating remained after annealing at 300 °C.

Table 2. Stages in the Thermal Annealing of the Glass-Ceramic Gratings

Annealing Stage	Annealing Temperature (°C)	Annealing Duration (h)
0	20	—
1	100	5
2	100	86
3	200	18
4	300	18
5	400	19½
6	500	21¾

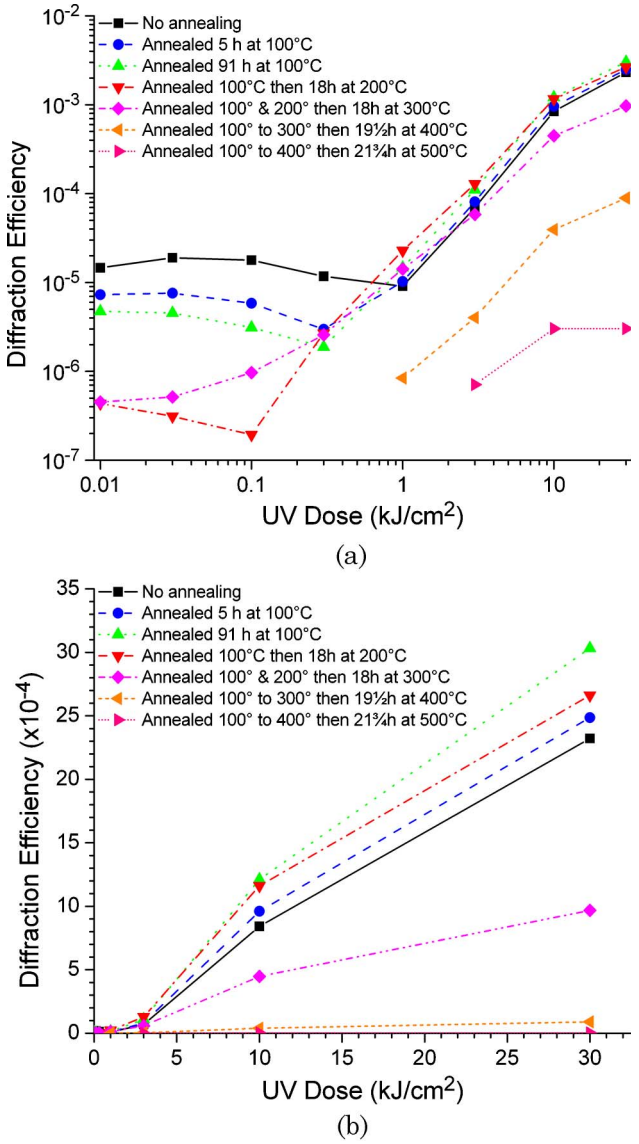

Fig. 4. (Color online) Bragg diffraction efficiency versus UV dose for a grating written at 248 nm and subsequently annealed at various temperatures. (a) Log-log plot to emphasize effects at a low-UV dose. (b) The same data plotted on linear axes to emphasize the effects at a high-UV dose.

For the high-UV-dose regime, the annealing behavior is markedly different. Figures 4(b) and 5 show that the high-UV-dose gratings actually *increase* in strength when annealed at 100 °C. For example, after annealing for 91 h at 100 °C, the diffraction efficiency increases from 2.3×10^{-3} to 3.0×10^{-3}, or equivalently Δn increases from 5.6×10^{-5} to 6.4×10^{-5}. Beyond 200 °C, the strength of these high-exposure gratings rolls off approximately exponentially with temperature. We see that some remnant of the high-exposure gratings remains detectable even after annealing at 500 °C.

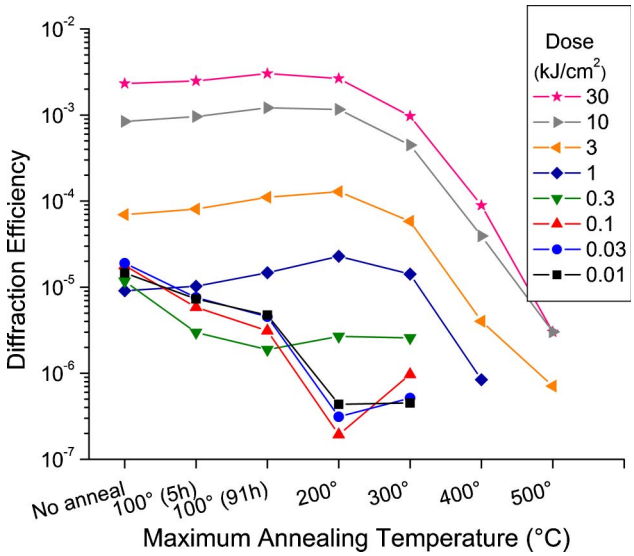

Fig. 5. (Color online) Bragg diffraction efficiency versus annealing temperature for a grating written at 248 nm. This figure presents an alternative view of the same data as Fig. 4.

4. Optical Absorption Measurements

We looked for evidence of physical change in the WMS-15 glass ceramic under UV irradiation by measuring the change in optical absorption of the material following 248 nm irradiation. We irradiated 3.07 mm thick samples of the glass ceramic using an unpatterned beam to give the same average exposure doses as were used in the writing of the gratings. The exposures were performed at 100 pulses per second, using the KrF excimer. The absorption spectra were measured from 250 to 900 nm using a dual-beam spectrometer. Figure 6 shows the optical absorption spectra for a nonirradiated sample, and for UV energy doses of 0.03 and 30 kJ/cm^2.

When we converted the measured absorption data to absorbance in dB/cm (defined as $-10\log_{10}(\tau)$, where τ is the internal transmittance), we assumed uniform absorbance through the 3.07 mm thickness of the sample. However, for the spectra following irradiation at 248 nm, this assumption is not justified as the penetration depth of the 248 nm light is much less than the sample thickness. Therefore, in subsequent graphs, we plot differences in optical absorbance in decibels, not decibels per unit length.

The differences between the absorption spectra in Fig. 6 are difficult to see. Close examination of the spectra reveals that the increase in absorption behaves differently for the low- and high-dose exposures. This can be described as a shift to longer wavelength of the tail of the UV absorption feature. Therefore, as an aid to more detailed visualization of the behavior, we averaged the absorption data over four wavelength bands, 265 to 299 nm (far UV), 300 to 349 nm (mid UV), 350 to 399 (near UV), and 400 to 700 nm (visible). The *increase* in absorbance as a function of UV exposure dose for each of these bands is plotted in Fig. 7.

In the far UV (squares), there is a steady increase of absorbance increase with irradiation dose. In the visible- (apex-down triangles) and near-UV (apex-up triangles) wavelength bands, there is a rapid rise then a fall in absorbance change for fluences between 0.01 and 1 kJ/cm^2, followed by a reduced, very slow increase of absorbance change with increasing fluence for exposures above 1 kJ/cm^2. The demarcation between low dose (less than 1 kJ/cm^2) and high dose (1 kJ/cm^2 and above) occurs at precisely the same doses as the change in grating diffraction efficiency seen in Figs. 1 and 4. This observation links the photoinduced index change and the change in optical absorption, and also supports a hypothesis that

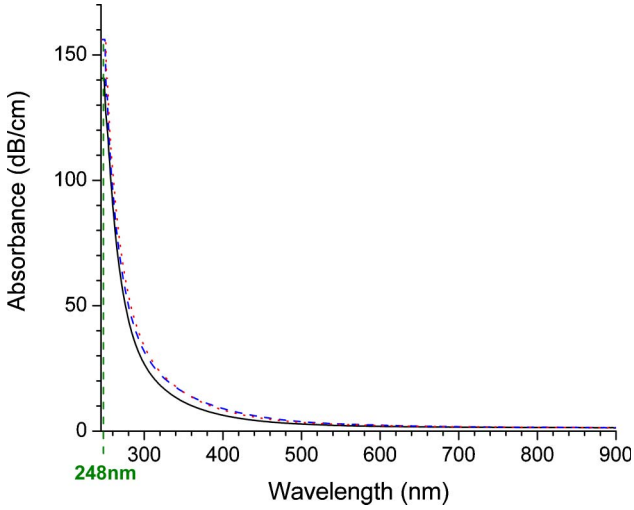

Fig. 6. (Color online) Optical absorption spectra for a 3 mm thick WMS-15 glass-ceramic slab. Three spectra are shown: unprocessed sample (solid curve), 0.03 kJ/cm^2 exposed sample (dashed curve), and 30 kJ/cm^2 exposed sample (dotted curve). In this representation, the low- and high-UV dose spectra are almost indistinguishable. The dashed vertical line at 248 nm marks the UV exposure wavelength.

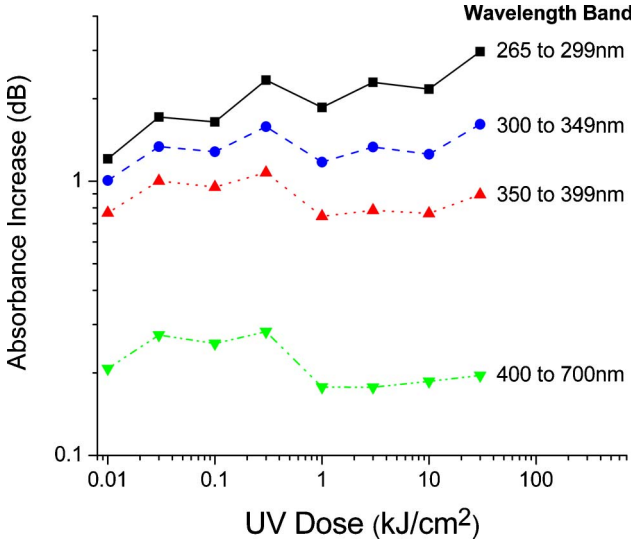

Fig. 7. (Color online) Optical absorption *increase* due to 248 nm exposure as a function of the UV dose. The four curves represent spectral data averaged over the indicated wavelength bands.

different physical changes in the glass are responsible for the low-dose and high-dose grating formation.

From the measured absorption spectra we calculated the $1/e$ intensity absorption depth of the glass ceramic at 248 nm. The results for unexposed, weakly exposed, and strongly exposed samples are summarized in Table 3.

From the absorption depth values in Table 3 we see that the average absorption depth during writing of the low-dose $0.03\,\mathrm{kJ/cm^2}$ grating was somewhere between 299 and 264 μm, resulting in a grating whose thickness is about 160 μm.

For the visible wavelength band, the curve in Fig. 7 agrees with the visual observation that the glass ceramic was noticeably darkened, with the maximum darkening occurring for exposures between 0.03 and $0.3\,\mathrm{kJ/cm^2}$.

The measured optical absorption of an unprocessed glass-ceramic sample at the probe wavelength of 633 nm is 0.159 dB for a 3 mm thickness. The corresponding absorbance is $\alpha_0 = 0.519\,\mathrm{dB/cm}$. After uniform irradiation with 248 nm light at $0.03\,\mathrm{kJ/cm^2}$, the measured *increase* in optical absorption for a 3 mm thick sample was 0.10 dB. Since the absorption depth at 248 nm is $264 \pm 10\,\mu$m (see Table 3), we will make the simplifying assumption that the entire 0.10 dB increase in absorption occurs over this distance, corresponding to an additional absorbance of $\Delta\alpha_{uv} = 0.10/(264 \times 10^{-4}) = 3.79\,\mathrm{dB/cm}$. When the sample is exposed through a phase mask, the peaks of the fringe pattern will be exposed to twice the uniform illuminating fluence. If we make another simplifying assumption that the UV-induced optical absorption is proportional to the fluence, then the increase in absorbance at the bright fringe peaks is $2\Delta\alpha_{uv}$. An absorption grating is thus formed, with an average absorbance of $\alpha_{av} = (\alpha_0 + \Delta\alpha_{uv})$, and an absorption modulation depth of $\Delta\alpha_{uv}$. Kogelnik [30] shows that, in mixed refractive index and absorption gratings, the two diffractive mechanisms can be treated additively, and the diffraction efficiency of the absorption grating is given by his Eq. 50:

$$\eta_{abs} = \exp\left(\frac{-2\alpha_{av}d}{\cos\theta_B}\right) \times \sinh^2\left(\frac{\Delta\alpha_{uv}d}{2\cos\theta_B}\right). \qquad (4)$$

Table 3. Measured Absorption Depth at 248 nm and Grating Thickness for Unexposed, Weakly Exposed, and Strongly Exposed Glass-Ceramic Samples[a]

UV Exposure Dose ($\mathrm{kJ/cm^2}$)	$1/e$ Intensity Absorption Depth (μm)	Grating Thickness (μm)	Grating Modulation
0	299	—	
0.03	264	160	Absorption loss
30	245	127	Refractive index

[a]We estimate uncertainties of $\pm 10\,\mu$m in the absorption depth and $\pm 20\,\mu$m in the grating thickness.

Substituting the numerical values above for α_{av} and $\Delta\alpha_{uv}$ and taking $d = 264$ and $\theta_B = 45.57°$, we calculate $\eta_{abs} = 4.6 \times 10^{-5}$. From the data in Fig. 5, we see that, for an unannealed grating written at $0.03\,\mathrm{kJ/cm^2}$, the measured diffraction efficiency is 1.9×10^{-5}. What we can conclude from this is that the observed diffraction behavior, for a weakly exposed grating such as this, can feasibly be attributed to the UV-induced increase in optical absorption at the visible probe wavelength. There is no need to invoke any contribution from a refractive index modulation or a surface relief grating. The discrepancy between the calculated absorption grating diffraction efficiency and the measured diffraction efficiency can easily be accounted for by the oversimplistic assumptions that went into the calculated value.

On the other hand, when a glass ceramic was exposed to uniform UV illumination at the relatively high fluence of $30\,\mathrm{kJ/cm^2}$, we measured an increase in optical absorption of 0.08 dB. If we assume that absorption increase happens only over a thickness $d = 127\,\mu$m (see Table 3) because of light–matter interactions at high fluences, then the increase in absorbance is $\Delta\alpha_{uv} = 6.30\,\mathrm{dB/cm}$. In this case, Kogelnik's Eq. 50 [30] gives $\eta_{abs} = 3.2 \times 10^{-5}$. The measured diffraction efficiency is 2.3×10^{-3}, which is almost 2 orders of magnitude larger. We still need to consider the possibility that a surface relief grating contributes to the measure diffraction efficiency. Surface relief gratings have been reported in several glass compositions, such as tin codoped [31] and lead silicate [32]. Thicknesses of such gratings are typically in the range of 5 [31] to 70 nm [32]. These thin surface relief gratings would display a very low sensitivity to angular offset from the Bragg condition of the probe beam. The fact that we do not observe a significant broad pedestal in the angular offset data in Fig. 2 is strong evidence that a surface relief grating does not play a significant role in the observed diffraction from a strong grating. Therefore, neither absorption nor surface relief gratings appears to play a significant role in the observed diffraction from high-UV fluence gratings in WMS-15 glass ceramic.

The uniformly exposed glass-ceramic samples were annealed for 18 h at 200 °C and their absorption spectra were remeasured. Figure 8 shows the *decrease* in optical absorbance of the exposed samples caused by annealing at 200 °C.

It is worth emphasizing that the quantity on the vertical axis in Fig. 8 is the *reduction* of optical absorbance caused by the thermal annealing. The great similarity between Fig. 7 (absorption *increase* caused by UV exposure) and Fig. 8 (absorption *decrease* due to subsequent annealing at 200 °C) shows that the majority of the absorption increase caused by exposure is erased by the annealing. In particular, for visible wavelengths, the net absorbance change after the complete exposure–annealing cycle was less than 0.10 dB for all exposure doses.

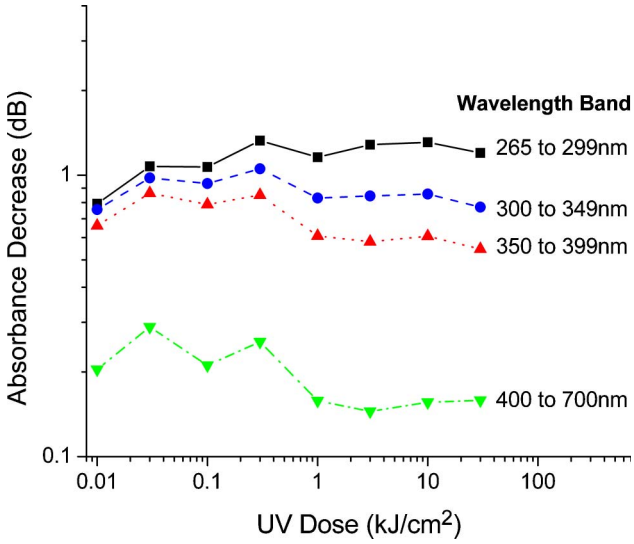

Fig. 8. (Color online) Optical absorption *decrease* due to thermal annealing at 200 °C of samples that had previously been exposed at 248 nm. As in Fig. 7, the four curves represent spectral data averaged over the indicated wavelength bands.

5. Discussion

There is clear evidence presented above for two distinct photosensitivity mechanisms that are responsible for the inscription of gratings in the WMS-15 glass ceramic. These are summarized in Table 4.

Unfortunately, we do not know the exact physical and chemical composition of WMS-15 (which is a trade secret), so it was not possible for us to attribute the effects of UV exposure to specific structures or constituents in the manner of studies such as those of Livingston *et al.* [19] or the stress studies of Zwanziger *et al.* [33]. However, analysis of the net change in absorption spectrum caused by 248 nm exposure followed by annealing at 200 °C does reveal a broad feature, centered at about 360 nm, which is apparent only for exposures between 0.01 and 0.3 kJ/cm^2. This feature is clearly visible in Fig. 9.

We speculate that the formation of absorption loss gratings at low-UV doses, which shows low thermal stability, may be associated with absorption by color center defects. At high-UV doses, even after annealing at 500 °C, the short wavelength absorption has still not recovered to its initial value. This observation leads us to suggest that the more thermally stable high-UV dose induced index change may be related to the shift in the UV absorption edge that we see in Figs. 6 and 9. A more detailed study of the mechanisms of the photosensitivity will be the subject of future work.

One of the exciting features of glass ceramics is the wide range of thermal expansion coefficients and thermo-optic coefficients. If a suitable combination of these parameters can be obtained in a material, it is possible, in principle, to create grating structures that are insensitive to temperature, at least over a given range of temperatures and wavelengths. The first-order Bragg wavelength of a grating is given by

$$\lambda_B = 2n\Lambda, \tag{5}$$

where n is the average effective index. We can calculate the fractional temperature-dependent change in the Bragg wavelength by differentiating Eq. (5) to give

$$\Delta\lambda_B = \frac{1}{\lambda_B}\frac{d\lambda_B}{dT} = 2\frac{\Lambda}{\lambda_B}(\xi + n\alpha), \tag{6}$$

where $\alpha = (1/\Lambda)(d\Lambda/dT)$ is the linear coefficient of thermal expansion and $\xi = dn/dt$ is the thermo-optic coefficient. We have neglected any additional change in index caused by the stress optic effect. We substitute the values of the thermal coefficients for WMS-15 [28], $n = 1.524$ at a wavelength of 1550 nm, $\alpha = 11.4 \times 10^{-6}/°C$, and $\xi = -2.1 \times 0^{-6}/°C$ into Eq. (6) to give $\Delta\lambda_B = 9.9 \times 10^{-6}/°C$. The temperature sensitivity of Bragg wavelength for a grating of

Table 4. Summary of Differences Between Low-Energy-Dose and High-Energy-Dose Changes in WMS-15 Glass Ceramic Exposed at 248 nm

Parameter	Low-UV Dose	High-UV Dose
Energy dose range (kJ/cm^2)	<1	≥1
Dose for maximum grating strength (kJ/cm^2)	~0.3	>30
Grating mechanism	Absorption loss modulation	Refractive index modulation
Grating growth rate	Rapid up to maximum, then negative	Slow increase
Grating thickness (μm)	160 ± 20	127 ± 20
Effect of annealing	Decrease in strength	Increase in strength up to ~200 °C, then decrease
Temperature for 50% erasure of index or absorbance modulation (°C)	~100	~300
Change in visible wavelength absorbance with UV dose	Peaks at about 1 kJ/cm^2, then decreases for higher exposure	Increases very slowly with exposure
Change in visible wavelength absorbance with annealing at 200 °C	Bleaches rapidly	Little change
Change in UV wavelength absorbance with UV dose	Increases slowly with exposure	Increases very slowly with exposure
Change in UV wavelength absorbance with annealing at 200 °C	Decreases slowly with exposure	Little change

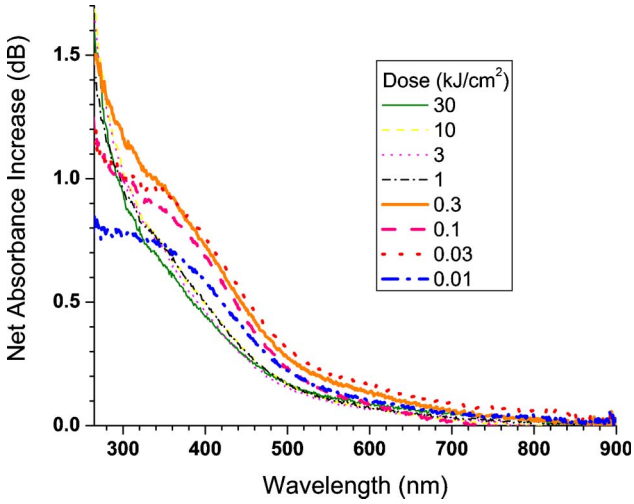

Fig. 9. (Color online) Spectra of total absorption increase due to UV exposure at 248 nm, followed by annealing at 200 °C. The thick curves show low-UV dose spectra and the thin lines are the high-UV dose spectra.

period 500 nm in WMS-15 would be 1.5 nm/°C. Since this value is not very different from the corresponding value for typical germanosilicate glass waveguides, we conclude that the Ohara WMS-15 glass ceramic does not offer a significantly decreased temperature sensitivity, despite its negative thermo-optic coefficient. This finding does not rule out the possibility of finding an existing transparent glass-ceramic material, or creating a new material with thermal properties that would result in a much decreased thermal sensitivity.

6. Conclusions

We have demonstrated for the first time, to our knowledge, the UV inscription, without subsequent chemical etching or thermal development, of thick diffraction gratings in a glass-ceramic material. Grating strength, thermal annealing, and optical absorption measurements support the hypothesis that two different physical mechanisms are involved in the photoinduced changes in the properties of the glass-ceramic material, according to whether the total exposure is less or greater than about $0.3\,\mathrm{kJ/cm^2}$. For lower fluences, gratings are predominantly formed by absorption loss modulation, while at higher fluences, gratings result from more thermally stable refractive index modulation. High-fluence gratings written with UV wavelengths of 248 and 193 nm achieved refractive index changes greater than 5×10^{-5}, with indication that substantially larger changes are possible with higher energy doses.

The authors thank Viscore Technologies for proposing and supporting this work, and for supplying the Ohara WMS-15 glass-ceramic samples. J. Albert acknowledges support from the Canada Research Chairs program. This work is partially supported by the Natural Sciences and Engineering Research Council of Canada (NSERC). We also thank A. Ianoul and G. Galway from the Department of Chemistry at Carleton University for providing access to the UV–visible spectrometer. The authors are grateful to the anonymous reviewer, whose comments led us to consider absorption loss modulation as the mechanism for the low-fluence gratings.

References

1. W. Höland and G. Beall, *Glass Ceramic Technology* (American Ceramic Society, 2002).
2. M. Brinkmann, J. Hayden, M. Letz, S. Reichel, C. Click, W. Mannstadt, B. Schreder, S. Wolff, S. Ritter, M. J. Davis, T. E. Bauer, H. Ren, Y.-H. Fan, S.-T. Wu, K. Bonrad, E. Krätzig, K. Buse, and R. A. Paquin, "Optical materials and their properties," in *Springer Handbook of Lasers and Optics*, F. Träger, ed. (Springer, 2006), pp. 300–306.
3. C. N. Chu, N. Saka, and N. P. Suh, "Negative thermal expansion ceramics: a review," Mater. Sci. Eng. **95**, 303–308 (1987).
4. D. L. Weidman, G. H. Beall, K. C. Chyung, G. L. Francis, R. A. Modaavis, and R. M. Morena, "A novel negative expansion substrate material for athermalizing fiber Bragg gratings," in *Proceedings of 22nd European Conference on Optical Communication* (1996), Vol. 1, paper MoB.3.5, pp. 61–64.
5. H. Bach and D. Krause, *Low Thermal Expansion Glass Ceramics* (Springer, 2005).
6. N. Goto, M. Kataoka, and D. G. Polensky, "Glass-ceramics for a light filter," U.S. patent 6,677,259 (13 January 2004).
7. .H. Minamikawa, K. Ohara, and N. Goto, "Low expansion transparent glass-ceramics, glass-ceramic substrate and optical waveguide element," U.S. patent 7,148,164 (12 December 2006).
8. Y. Feng, J. Lu, K. Takaichi, K. Ueda, H. Yagi, T. Yanagitani, and A. A. Kaminskii, "Passively *Q*-switched ceramic Nd^{3+} : YAG/Cr^{4+} : YAG lasers," Appl. Opt. **43**, 2944–2947 (2004).
9. M. Ciofini and A. Lapucci, "Efficiency optimization for a diode-pumped Nd:YAG ceramic slab laser," Appl. Opt. **44**, 4388–4393 (2005).
10. A. Ikesue and V. L. Aung, "Ceramic laser materials," Nat. Photon. **2**, 721–727 (2008).
11. A. M. Malyarevich, I. A. Denisov, K. V. Yumashev, O. S. Dymshits, A. A. Zhilin, and U. Kang, "Cobalt-doped transparent glass ceramic as a saturable absorber *Q* switch for erbium:glass lasers," Appl. Opt. **40**, 4322–4325 (2001).
12. Y. V. Volk, A. M. Malyarevich, K. V. Yumashev, O. S. Dymshits, A. V. Shashkin, A. A. Zhilin, U. Kang, and K. Lee, "Influence of reducing-oxidizing conditions on the optical properties of Co^{2+}-doped magnesium aluminosilicate glass ceramics and their use as an effective saturable absorber *Q* switch," Appl. Opt. **43**, 6011–6015 (2004).
13. T. Erdogan, A. Partovi, V. Mizrahi, P. J. Lemaire, W. L. Wilson, T. A. Strasser, and A. M. Glass, "Volume gratings for holographic storage applications written in high-quality germanosilicate glass," Appl. Opt. **34**, 6738–6743 (1995).
14. R. Kashyap, *Fiber Bragg Gratings* (Academic, 1999).
15. A. Othonos and K. Kalli, *Fiber Bragg Gratings* (Artech House, 1999).
16. P. Jelger, P. Wang, J. K. Sahu, F. Laurell, and W. A. Clarkson, "High-power linearly-polarized operation of a cladding-pumped Yb fibre laser using a volume Bragg grating for wavelength selection," Opt. Express **16**, 9507–9512 (2008).
17. S. D. Stookey, "Photosensitive glass—A new photographic medium," Ind. Eng. Chem. **41**, 856 (1949).
18. P. D. Fuqua, S. W. Janson, W. W. Hansen, and H. Helvajian, "Fabrication of true 3D microstructures in glass/ceramic materials by pulsed UV laser volumetric exposure techniques," Proc. SPIE **3618**, 213–220 (1999).

19. F. E. Livingston, P. M. Adams, and H. Helvajian, "Active photo-physical processes in the pulsed UV nanosecond laser exposure of photostructurable glass ceramic materials," Proc. SPIE **5662**, 44–50 (2004).
20. F. E. Livingston and H. Helvajian, "Variable UV laser exposure processing of photosensitive glass-ceramics: maskless micro- to mesoscale structure fabrication," Appl. Phys. A **81**, 1569–1581 (2005).
21. L. B. Glebov and V. I. Smirnov, "Sensitization of photo-thermo-refractive glass to visible radiation by two-step illumination," U.S. patent 7,326,500 (5 February 2008).
22. M. Kösters, H.-T. Hsieh, D. Psaltis, and K. Buse, "Holography in commercially available photoetchable glasses," Appl. Opt. **44**, 3399–3402 (2005).
23. Y. Cheng, K. Sugioka, M. Masuda, K. Toyoda, M. Kawachi, K. Shihoyama, and K. Midorikawa, "3D microstructuring inside Foturan glass by femtosecond laser," RIKEN Rev. **50**, 101–106 (2003).
24. O. M. Efimov, L. G. Glebov, L. N. Glebova, K. C. Richardson, and V. I. Smirnov, "High efficiency Bragg gratings in photothermorefractive glass," Appl. Opt. **38**, 619–627 (1999).
25. N. Chiodini, A. Paleari, and G. Spinolo, "Photorefractivity in nanostructured tin-silicate glass ceramics: a radiation-induced nanocluster size effect," Phys. Rev. Lett. **90**, 055507 (2003).
26. N. Chiodini, A. Paleari, G. Spinolo, P. Crespi, "Photorefractivity in $SiO_2:SnO_2$ glass-ceramics by visible light," J. Non-Cryst. Solids **322**, 266–271 (2003).
27. A. Paleari, E. Franchina, N. Chiodini, A. Lauria, E. Bricchi, and P. G. Kazansky, "SnO_2 nanoparticles in silica: nanosized tools for femtosecond-laser machining of refractive index patterns," Appl. Phys. Lett. **88**, 131912 (2006).
28. "Glass-ceramic substrate for DWDM thin-film filter (WMS-15)" (Ohara Corporation), http://www.ohara-inc.co.jp/en/product/electronics/wms.html.
29. C. Ghio, Ohara Corporation (personal communication, 2008).
30. H. Kogelnik, "Coupled wave theory for thick hologram gratings," Bell Syst. Tech. J. **48**, 2909–2947 (1969).
31. M. Lancry, M. Douay, P. Niay, F. Beclin, Y. Menke, G. Milanese, M. Ferraris, and B. Poumellec, "Self induced gratings in ternary $SiO_2:SnO_2:NaO_2$ bulk glasses by UV light seeding," Opt. Express **13**, 6878 (2005).
32. X.-C. Long and S. R. Brueck, "Large photosensitivity in lead-silicate glasses," Appl. Phys. Lett. **74**, 2110–2112 (1999).
33. J. W. Zwanziger, U. Werner-Zwanziger, E. D. Zanotto, E. Rotari, L. N. Glebova, L. B. Glebov, and J. F. Schneider, "Residual internal stress in partially crystallized photothermorefractive glass: evaluation by nuclear magnetic resonance spectroscopy and first principles calculations," J. Appl. Phys. **99**, 083511 (2006).